Applied Surface Science 469 (2019) 34–43

Contents lists available at ScienceDirect

Applied Surface Science

journal homepage: www.elsevier.com/locate/apsusc

Full Length Article

Photocatalytic hydrogen production and photodegradation of organic dyes of hydrogenated TiO_2 nanofibers decorated metal nanoparticles

Ming-Chung Wu[a,*,b,c], Wei-Kang Huang[a], Ting-Han Lin[a], Yu-Jen Lu[d,e,*]

[a] Department of Chemical and Materials Engineering, Chang Gung University, Taoyuan 33302, Taiwan
[b] Green Technology Research Center, Chang Gung University, Taoyuan 33302, Taiwan
[c] Division of Neonatology, Department of Pediatrics, Chang Gung Memorial Hospital, Linkou, Taoyuan 33305, Taiwan
[d] Department of Neurosurgery, Chang Gung Memorial Hospital, Linkou, Taoyuan 33305, Taiwan
[e] College of Medicine, Chang Gung University, Taoyuan 33302, Taiwan

ARTICLE INFO

Keywords:
Hydrogenated TiO_2
Metal decorated TiO_2
Photodegradation
Photocatalytic hydrogen production

ABSTRACT

A series of metal decorated hydrogenated TiO_2 nanofibers (metal-H:TiO_2 NFs) are synthesized successfully in this study. It is synthesized by the hydrothermal approach and combined with wet impregnation method in thermal hydrogen reduction. Nine types of metal nanoparticles, Ag, Co, Cr, Cu, Fe, Ni, Pd, Pt and Y, were used to decorate on the surface of H:TiO_2 to enhance the photocatalytic activity. The photocatalytic performance of various metal-H:TiO_2 NFs was estimated by the photodegradation of organic dyes. Ag-H:TiO_2 NFs gives the fastest decoloration rate of brilliant green among others. Moreover, the evolution rate of H_2 over Pd-H:TiO_2 NFs under UV-A and UV-B illumination is 17,000 μmol/g·h and 25,600 μmol/g·h, respectively, which corresponding to photoefficiency values of ~7.54% and ~11.35%. The metal-H:TiO_2 NFs developed in this study can be a facile and environmentally friendly way for searching the high-performance photocatalysts in the field of environmental and energy issue.

1. Introduction

Titanium dioxide (TiO_2) has attracted broad research attention because of their applications in environmental pollution removal and photocatalytic hydrogen generation in the past few decades [1–13]. The one-dimensional titanate nanomaterials synthesized from TiO_2 powders in alkaline solutions has developed a new trend for the synthesis of TiO_2 for large-scale TiO_2-based nanofibers [14–20]. Nanofibers is much easier to achieve a percolated electrical network with elongated materials than regular nanoparticles. Furthermore, a bunch of nanofibers leads to the mechanical strength in tangled networks and shows the heavier entanglement with other nanoparticles [11,18,21–27].

Hydrogenated TiO_2 (H:TiO_2) exhibited strong visible light absorbance, a disordered surface enriched in trap states, and remarkably improved photocatalytic performance. The hydrogenation process for TiO_2 is usually obtained by annealing in a tube furnace filled with high-pressure hydrogen accompanied by a long calcination time. However, the progress in high-pressure and high-temperature conditions could be a danger for large-scale production [28,29]. Since hydrogenation process was used to fabricate hydrogenated TiO_2, many scientists used this method to modify the bandgap to expand absorption behavior, and H:TiO_2 has activated a lot of interest in photocatalytic hydrogen production [30–32]. Hydrogenation was demonstrated as a direct and effect approach to obtain high-performance H:TiO_2 nanotubes and nanowires for photocatalytic hydrogen evolution [33,34]. Moreover, through introducing surface defects (oxygen vacancy and Ti^{3+} interstitial defect) on the TiO_2 surface by hydrogenation process, it will result in the highly localized midgap states which could enhance the photocatalytic performance by the appropriate separation of electron and hole in black TiO_2 [35,36]. Many research groups also reported that H:TiO_2 has been applied in visible-light photocatalytic application, such as the photo-oxidation of organic compound and photocatalytic hydrogen production [37–40].

Noble metal decoration on TiO_2 surface is a convenient method to enhance the photocatalytic activity. The noble metal can enhance the light-induced exciton separation efficiently due to the large work function of noble metal including silver (Ag), gold (Au), iridium (Ir), palladium (Pd), platinum (Pt), rhodium (Rh), and ruthenium (Ru), which can form Schottky barrier between TiO_2 and metal nanoparticles [41–49]. For certain metal nanoparticles can induce localized surface plasmon resonance. It increases the absorption of TiO_2 at certain wavelengths depend on the metal types [50–57]. Specific metals and metal

* Corresponding authors
E-mail addresses: mingchungwu@cgu.edu.tw (M.-C. Wu), alexlu0416@gmail.com (Y.-J. Lu).

https://doi.org/10.1016/j.apsusc.2018.10.240
Received 10 August 2018; Received in revised form 21 October 2018; Accepted 29 October 2018
Available online 30 October 2018
0169-4332/

oxides decorated on TiO_2 surface is an efficient approach to synthesize high activity TiO_2-based photocatalysts.

As photocatalytic science and technology has been widely developed in recent decades, doping noble metals on TiO_2 photocatalysts has been proved that specific interface between noble metals and TiO_2 can enhance the activity. Nevertheless, the H:TiO_2 photocatalytic property based on different metal NPs has not been revealed and discussed thoroughly. Which metal decorated on H:TiO_2 NFs surface perform the high photocatalytic performance on photodegradation of organic dye and photocatalytic hydrogen production is still unknown at this stage. Herein, in order to combine the merits of hydrogenated TiO_2 and noble metal decoration and enhance the photocatalytic performance, we explored the application of H:TiO_2 by integrating metal NPs on its surface.

In this study, various metal decorated hydrogenated TiO_2 nanofibers (metal-H:TiO_2 NFs) were synthesized by combining the hydrothermal process and wet-impregnation method, followed by one-step thermal treatment in low H_2 partial pressure. The optimal calcination condition is achieved to enhance the photocatalytic performance. A series of metal-H:TiO_2 NFs were applied for degradation of hazardous organic dye and photocatalytic hydrogen evolution under UV irradiation and discussed in detail. The developed metal-H:TiO_2 NFs could be a potential material in the fields of environmental pollutants removal and photocatalytic hydrogen production. Here, we report on the synthesis of H:TiO_2 NFs and their metal (Ag, Co, Cr, Cu, Fe, Ni, Pd, Pt, and Y)-decorated derivatives. To the best of our knowledge, Pd-H:TiO_2 NFs presents an outstanding H_2 evolution performance in water-ethanol solutions under UV-A and UV-B illumination [45].

2. Experimental details

The hydrogen sodium titanate nanofibers ($H_xNa_{2-x}Ti_3$ NFs) is prepared according to our previous study [58]. Nine types of metal precursors were used to decorate on the surface of $H_xNa_{2-x}Ti_3O_7$ NFs. For the 1.0 wt% metal decoration, 9.5 mg of silver nitrate ($AgNO_3$, CHONEYE, extra pure reagent), 30.2 mg of cobalt (II) nitrate hexahydrate ($Co(NO_3)_2{\cdot}6H_2O$, ACROS, 99%), 44.5 mg of chromium(III) nitrate nonahydrate ($Cr(NO_3)_3{\cdot}9H_2O$, ACROS, 99%), 25.5 mg of copper(II) acetylacetonate ($Cu(C_5H_7O_2)_2$, ACROS, 98%), 44.7 mg of iron(III) nitrate nonahydrate ($Fe(NO_3)_3{\cdot}9H_2O$, ACROS, 98 + %), 30.3 mg of nickel (II) nitrate hexahydrate ($Ni(NO_3)_2{\cdot}6H_2O$, ACROS, 99%), 12.8 mg of palladium (II) acetate ($Pd(OCOCH_3)_2$, ACROS, 99.9%), 12.5 mg of platinum (II) acetylacetonate ($Pt(C_5H_7O_2)_2$, ACROS, 98%) and 26.1 mg of yttrium(III) nitrate hexahydrate ($Y(NO_3)_3$, ACROS, 99.9%) were firstly dissolved in 200 mL of ethanol/acetone (1:1, v/v), separately. Then, 594 mg of $H_xNa_{2-x}Ti_3O_7$ NFs was suspended in the precursor solution using 3 h of ultrasonic agitation. The mixture of various metal precursors and $H_xNa_{2-x}Ti_3O_7$ NFs were stirred for 6 h, respectively. After evaporating the solvent at ~80 °C under N_2 atmosphere, the samples were undergo a calcination treatment in 15% H_2 (in N_2 buffer) flow for 12 h to obtain the various metal decorated hydrogenated TiO_2 nanofibers (metal-H:TiO_2 NFs). The illustration of the preparation of pristine TiO_2 NFs, H:TiO_2 NFs and various metal-H:TiO_2 NFs is shown in Fig. 1. The metal loading is ~1.0 wt% for each metal-H:TiO_2 NFs.

Absorption spectrophotometer (JASCO, V-650, Japan) is used to acquire the UV–Vis reflectance spectra of synthesized materials. X-ray diffractometer (Bruker, D2 phaser with Xflash 430) was used to determine the crystal structures of the synthesized materials using Cu K_α radiation at 50.0 kV and 300.0 mA. XRD patterns were collected from 2θ between 10 and 80 with a 0.005° step at 5° min^{-1}. For Raman scattering spectra of the TiO_2-based materials and the commercial anatase TiO_2 powder (Acros, 98 + %, anatase powder), they were positioned on a high-resolution piezoelectric stage of the scanning microscopy (WiTec, Alpha 300S) and were excited by a 632.8 nm He-Ne laser (25 mW). The laser beam was focused with a 10× objective lens (Nikon plane objective, NA ≈ 0.9), and the focused laser beam size was about 10 μm. Spherical-aberration corrected field-emission transmission electron microscope (JEOL, JEM-ARM200FTH, Japan) is adopted to investigate the microstructure of the synthesized materials.

Photodegradation activity was determined by evaluating the decolorization of brilliant green. First of all, 20.0 mg TiO_2 catalyst was dispersed in 150 mL of brilliant green solution (10.0 mg/L). After 30 min adsorption process in the dark to eliminate the deviation, the mixture solution was irradiated under two lamps of UV-A light and vigorously stirred at the same time. These specimens were centrifuged at 5000 rpm for 15 min to remove the remaining TiO_2 catalyst. The concentration of brilliant green in the supernatant was quantified at the absorbance of $\lambda = 624$ nm by UV–Vis spectrophotometer (Jasco Analytical Instruments, V-650 UV–Vis Spectrophotometer) and further calculated based on Beer-Lambert law. On the other hand, photocatalytic hydrogen production was conducted in the home-made system under UV-B and UV-A irradiation.[59] 10.0 mg TiO_2 catalyst was dispersed in 2.0 L mixture of ethanol and water which volumetric ratio is 1:1. For the photostability of the TiO_2 catalysts, the photocatalytic hydrogen production was performed in five cycles via the same condition and parameter. To study the photoelectrochemical properties, the linear sweep voltammetry (LSV), transient photocurrent, and electrical impedance spectroscopy (EIS) were analyzed by a potentiostat (Metrohm, Autolab PGSTAT302N) with a standard three-electrode system including Ag/AgCl in KCl as a reference electrode, Pt counter electrode, and TiO_2-coated working electrode. 0.50 M sodium sulfate aqueous solution was used as electrolyte. The 1.0 cm^2 TiO_2 electrode was fabricated via blade coating method to lie the paste on the FTO, which paste consisted of 0.10 g TiO_2 catalyst, 2.50 mL ethanol, 0.50 mL water and few Triton X-100 (Sigma-Aldrich). The pristine TiO_2 electrode was calcined at 350 °C for 3 h in the air, while H:TiO_2 and metal-H:TiO_2 electrode were calcined at 350 °C for 3 h in the air followed by thermal reduction in the 15% H_2 (in N_2 buffer). For the LSV measurement, applied potential ranged from −0.5 to 1.5 V with scan rate of 50 $mV{\cdot}s^{-1}$. The transient photocurrent was detected with a potential of 0 V. In the EIS, the potential was set as 0 V with an amplitude of 0.01 V, and frequency ranged from 1 to 10^4 Hz.

3. Results and discussion

The various TiO_2-based nanofibers calcined at different combinations of temperature and time are prepared to find the optimal calcination process for high-performance photocatalyst. The TiO_2 nanofibers calcined in air and in the flow of H_2/N_2 at various temperatures for 12 h are denoted as TiO_2-X NFs and H:TiO_2-X NFs respectively, for which "X" indicating the calcination temperature. Photos of pristine TiO_2 NFs and H:TiO_2 NFs calcined from 450 °C to 700 °C are shown in Fig. 2a and b. The pristine TiO_2 NFs calcined in air shows white color, but H:TiO_2 NFs calcined in the flow of H_2/N_2 is black. H:TiO_2-NFs and pristine TiO_2 NFs calcined below 450 °C could show the existence of carbon. Therefore, TiO_2 nanocrystals calcined above 450 °C are adopted for further study. From Fig. 2c and d, we can observe that the reflectance spectra clearly enhance in the visible region, when H:TiO_2 NFs is calcined in the flow of H_2/N_2 mixture. For H:TiO_2 NFs, the reflectance spectra reveal an enhancement compared with pristine TiO_2 NFs due to the oxygen atom defects and/or trivalent titanium formation [60].

The phase transformation and vibrational modes of the pristine TiO_2 NFs and H:TiO_2 NFs with various calcination temperatures are investigated by Raman scattering spectroscopy. From Fig. 3, Raman scattering spectra show that H:TiO_2 NFs transform to pure TiO_2 anatase phase when calcination temperature of 650 °C is reached. Raman spectra of anatase TiO_2 powder (Acros, 98 + %) was measured as the standard for structural identification. Anatase TiO_2 powder shows the six Raman-active modes, including E_g (144 cm^{-1}), E_g (200 cm^{-1}), B_{1g} (398 cm^{-1}), A_{1g} (515 cm^{-1}), B_{1g} (517 cm^{-1}), and E_g (640 cm^{-1}), of anatase phase, respectively [61]. For TiO_2-based material, there is an increased crystallinity as calcination temperature is raised. At the same calcination temperature, the signal of E_g band at 144 cm^{-1} of H:TiO_2

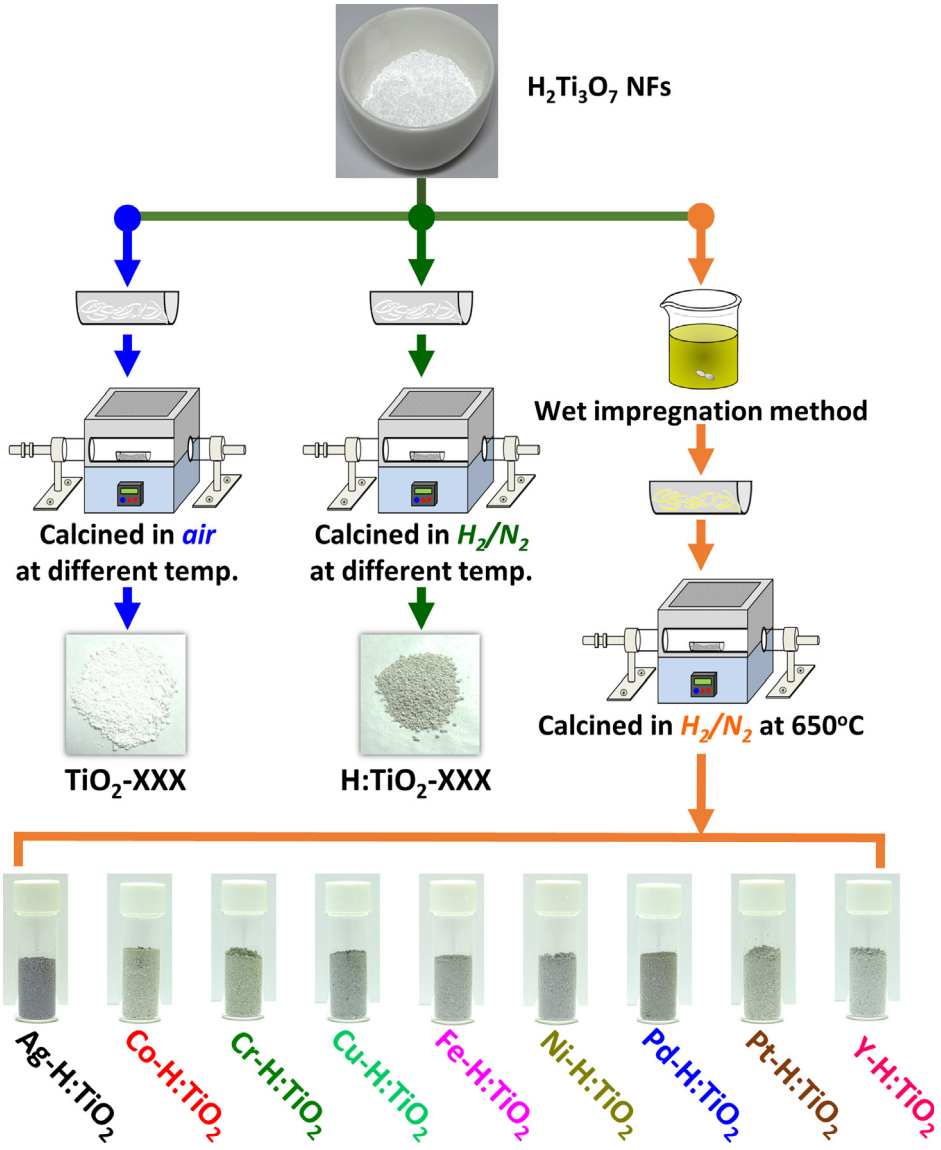

Fig. 1. Illustration of the preparation of pristine TiO_2 NFs, H:TiO_2 NFs and various metal-H:TiO_2 NFs.

NFs is weaker than pristine TiO_2 NFs, because the titanium trivalent ion and oxygen vacancies formation could be introduced through the calcination process in H_2/N_2 [28,60].

The crystal structure analysis for pristine TiO_2 NFs series and H:TiO_2 NFs series are characterized using X-ray diffractometer. The XRD patterns of TiO_2 NFs under the calcination procedure in the flow of H_2/N_2 are shown in Fig. 4. Below the calcination temperature of 650 °C, the intensity of (1 0 1) reflection at 2θ of 25.3° for H:TiO_2 NFs is increased with ascending the calcination temperature which is due to the high-temperature calcination process could improve the lattice ordering of anatase TiO_2. However, pristine TiO_2 NFs and H:TiO_2 NFs would transform to rutile phase TiO_2 at the calcination temperature of 700 °C. The intensity of (1 0 1) reflection at 2θ of 25.3° is thus decreased. For H:TiO_2 NFs series, the sample with the calcination temperature of 650 °C (H:TiO_2-650 NFs) exhibits a high degree of crystallinity with the crystalline phase anatase TiO_2. The H:TiO_2-650 NFs pattern could be indexed as the body-centered tetragonal unit cell of anatase TiO_2 [COD ID:720675]. The XRD study is in accordance with the Raman measurement. Hence, we adopted the calcination temperature of 650 °C to prepare the samples for further study.

The enhancement of photocatalytic activity gained through the hydrogenated procedure is revealed by photodegradation test of brilliant green under UV-A irradiation. To analyze the photodegradation performance, the retain concentration of brilliant green is calculated according to a calibration curve measured at λ = 625 nm in the absorption spectra. The photodegradation of brilliant green over H:TiO_2 follows first-order kinetics which is simplified from Langmuir-Hinshelwood kinetics at lower initial organic dye concentration. The kinetic constant, k, can be defined as $\ln\left(\frac{C}{C_0}\right) = -kt$; where C_0 and C represent the concentration of brilliant green at initial and time t, respectively, and k is the apparent reaction rate constant [4,62]. The photodegradation of brilliant green ($\frac{C}{C_0}$ curves) at various times over pristine TiO_2-650 NFs and various H:TiO_2 NFs and are shown in Fig. 5. Linearized kinetic plots of $\ln\left(\frac{C}{C_0}\right)$ versus t for photodegradation of brilliant green indicates the results are in good agreement with the Langmuir-Hinshelwood model (Fig. 5b). The linear slopes for each H:TiO_2 represent k, the reaction rate constant, which directly reveals the performance of photodegradation. Among pristine TiO_2 NFs series, pristine TiO_2-650 NFs shows the fastest decolorization rate for the photodegradation test, and its calculated reaction rate constant is $\sim 0.097\ min^{-1}$. Interestingly, H:TiO_2-650 NFs exists the highest calculated reaction rate constant of $\sim 0.111\ min^{-1}$ (Fig. 5c).

We demonstrate HRTEM study to reveal why H:TiO_2 shows high

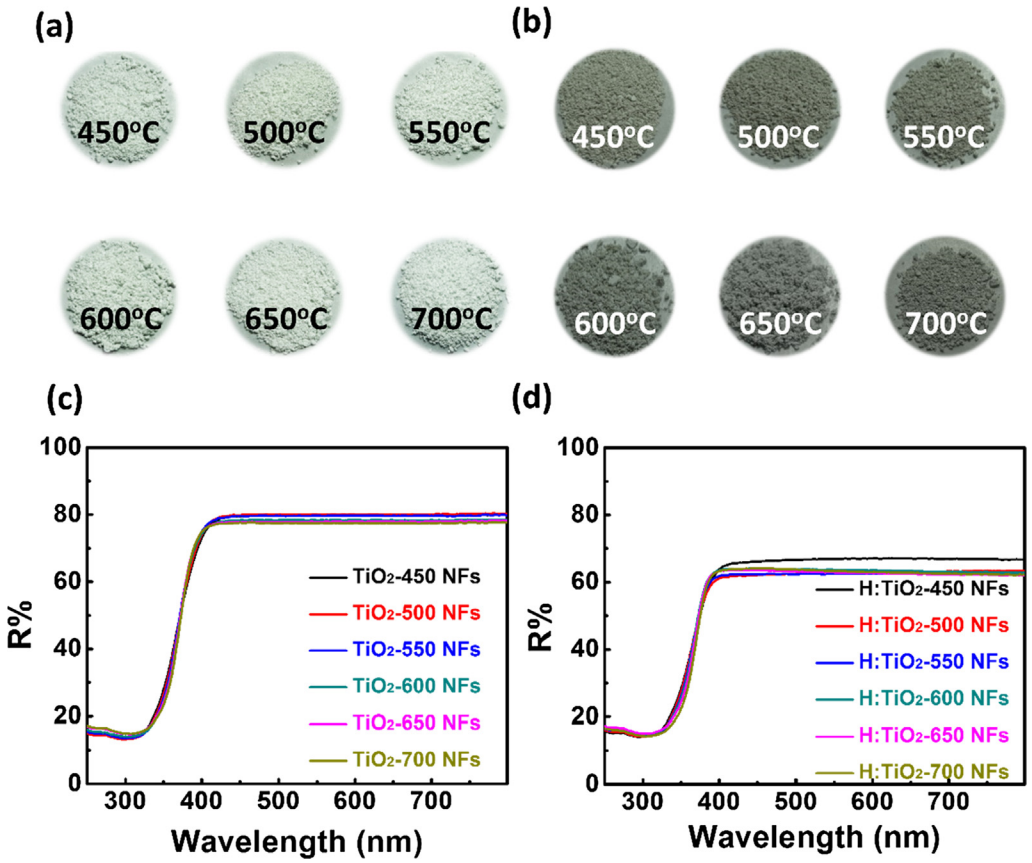

Fig. 2. (a, b) Photographs and (c, d) reflectance spectra of pristine TiO_2 NFs series (a, c) and H:TiO_2 NFs series (b, d) calcined at various temperatures in the flow of H_2/N_2 for 12 h.

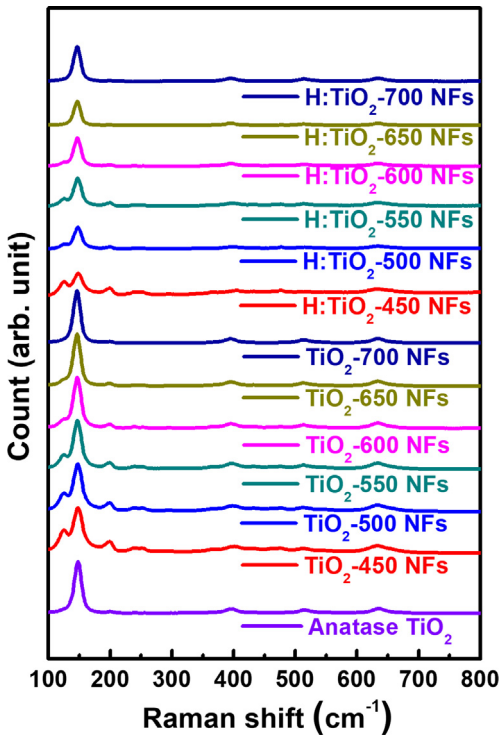

Fig. 3. Raman scattering spectra of pristine TiO_2 NFs series and H:TiO_2 NFs series calcined at various temperatures for 12 h and the commercial anatase TiO_2 powder.

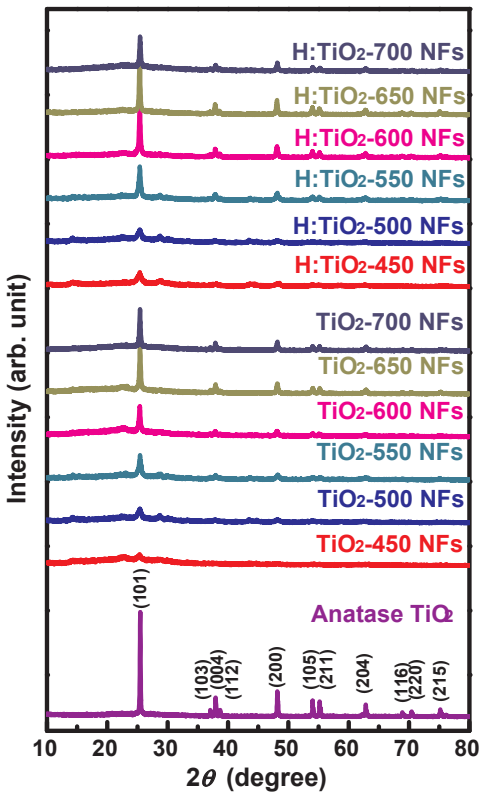

Fig. 4. XRD patterns of pristine TiO_2 NFs series and H:TiO_2 NFs series calcined at various temperatures for 12 h and the commercial anatase TiO_2 powder.

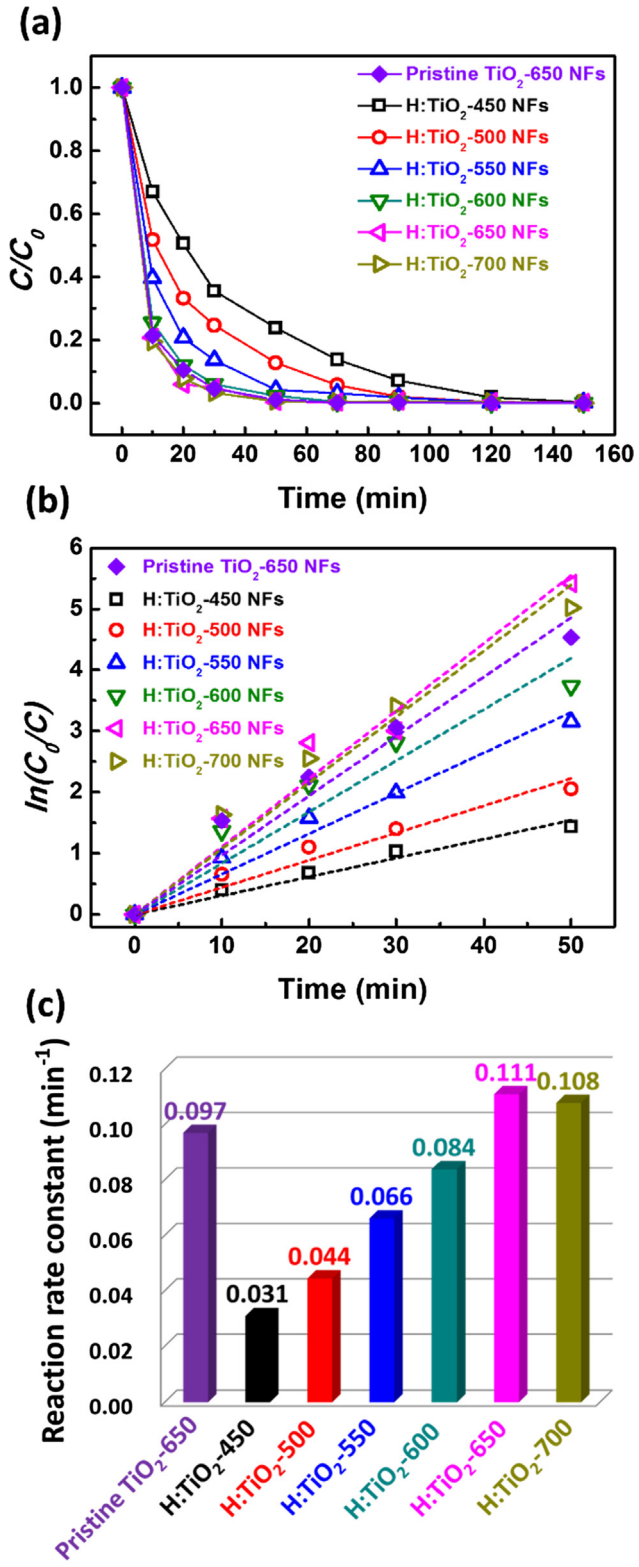

Fig. 5. (a) The C/C_o curves, (b) the linearized kinetic plots and (c) the reaction rate constants for the photodegradation of brilliant green using pristine TiO_2-650 and H:TiO_2 NFs series under UV-A irradiation.

performance in the photodegradation of brilliant green compared with pristine TiO_2-650 NFs (Fig. 6). The high-magnification lattice images are shown in Fig. 6b and d for pristine TiO_2-650 NFs and H:TiO_2-650 NFs, respectively. The insets of Fig. 6b and d shows the fast Fourier transformed patterns of both specimens for observing the direction of (1 0 1) crystal plane. The d_{101} of pristine TiO_2-650 NFs (3.50 Å) is larger than d_{101} of H:TiO_2-650 NFs (3.45 Å). The statements suggest that calcination in the flow of H_2/N_2 resulted in the oxygen vacancy, trivalent titanium (Ti^{3+}) and/or structural defect in the TiO_2 lattice. According to the literature, introducing the surface defect mentioned above on the surface of TiO_2 could impart the suppression of charge carrier recombination and enhanced optical absorption. Therefore, the excellent control of the microstructure can still warrant additional research effort from a materials science point of view.

Adding a proper co-catalyst is a facile method to activate the photodegradation performance and photocatalytic hydrogen production. Here, nine types of metal nanoparticles, Ag, Co, Cr, Cu, Fe, Ni, Pd, Pt, and Y, with a concentration of ~1.0 wt% are used to decorate on the surface of H:TiO_2-650 NFs. After the decoration procedure, the interface between the metal nanoparticle and TiO_2 would form a Schottky barrier which could facilitate the charge carrier transport. According to the mechanism of the photodegradation of organic dye, the more electron transfers to the surface could generate adequate reactive oxygen species (ROS) which seen as major factors for the photodegradation reaction [3]. The photodegradation test of brilliant green under UV-A irradiation is demonstrated here to reveal which of the metal nanoparticle could be a suitable candidate for enhancing the photocatalytic activity (Fig. 7). According to linearized kinetic plots fitted form $\left(\frac{C}{C_0}\right)$ curves (Fig. 7a and b), the Ag-H:TiO_2 NFs gives the fastest decolorization phenomenon. For the H:TiO_2 decorated with Ag, Pd, Pt and Y, they exhibit the faster decolorization phenomenon compared with nonmetal decorated H:TiO_2-650 NFs (~0.111 min^{-1}) over the photodegradation of brilliant green (Fig. 7c). The other metal decorated H:TiO_2-650 do not have suitable electronic properties for useful electron transfer reactions. The metal nanoparticles which negatively charged could lead to chemical reduction of protons on the surface; on the other hand, the metal nanoparticles which positively charged could enhance the oxidative process Herein, we proposed a possible photodegradation pathway shown as below [60,63].

$$\text{Metal-H:TiO}_2 + h\nu \rightarrow h^+ \text{ (H:TiO}_2\text{)} + e^- \text{(metal)} \quad (1)$$

$$O_2 + e^- \text{ (metal)} \rightarrow {}^{\cdot}O_2^- \quad (2)$$

$${}^{\cdot}O_2^- + H^+ \rightarrow {}^{\cdot}HO_2 \quad (3)$$

$$H_2O + h^+ \text{ (H:TiO}_2\text{)} \leftrightarrow OH^- \quad (4)$$

$$OH^- + h^+ \text{ (H:TiO}_2\text{)} \leftrightarrow {}^{\cdot}OH + H^+ \quad (5)$$

$${}^{\cdot}OH + \text{organic dye} \rightarrow \text{oxidation products} \quad (6)$$

$${}^{\cdot}HO_2 + \text{organic dye} \rightarrow \text{oxidation products} \quad (7)$$

As the metal-H:TiO_2 was irradiated by the light with sufficient energy, the electron-hole pairs will form and separate. The electrons will prefer to transfer through the defect area then to schottky barrier and finally into metal NPs; the holes will stay in the bulk TiO_2. Subsequently, a series of redox reaction occur and produce the several ROS such as ${}^{\cdot}O_2^-$, ${}^{\cdot}HO_2$, OH^-, and ${}^{\cdot}OH$. Finally, these radicals will oxide the organic dye and convert it to harmless products.

The photocatalytic hydrogen evolution of various metal-H:TiO_2 NFs are investigated under the UV-A and UV-B light irradiation, respectively. In Fig. 8a, both of Pd- and Pt-decorated on H:TiO_2 NFs present the excellent hydrogen production rates, which are ~9000 and 17,000 μmol/g·h under UV-A illumination. It means these two kinds of noble metal decoration are beneficial for achieving the high photocatalytic activity as illumination. Furthermore, the photocatalytic hydrogen production of as-prepared TiO_2 NFs irradiated by UV-B light are measured and the corresponding evolution rates are demonstrated in Fig. 8b. Interestingly, Ni-H:TiO_2 NFs also shows the ability to produce the hydrogen and its evolution rate is seen to be about 1900 μmol/g·h. Pt-H:TiO_2 NFs remains the similarly high rate of 14,900 μmol/g·h under UV-B illumination. Meanwhile, Pd-H:TiO_2 NFs exhibits the highest

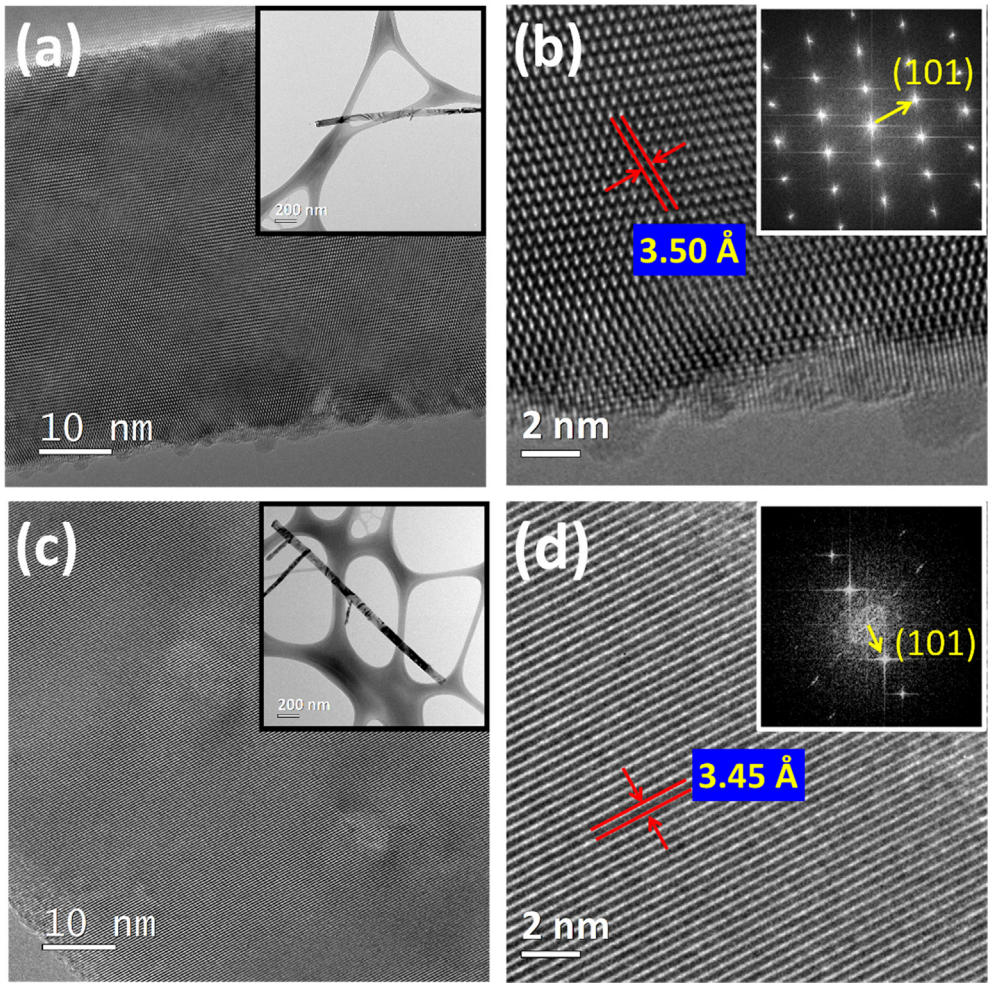

Fig. 6. HRTEM images of (a, b) pristine TiO_2-650 NFs and (c, d) H:TiO_2-650 NFs, and the insets of (b, d) are the corresponding fast Fourier transformed pattern of pristine TiO_2-650 NFs and H:TiO_2-650 NFs.

production rate at 25,600 μmol/g·h. After the five cycles, it still maintains ~72% of hydrogen evolution rate as shown in Fig. S1. In this case, the photocatalytic H_2 evolution over most metal-H:TiO_2 showed suppressed and low activities compared to photodegradation performance. As we know, photocatalytic H_2 evolution is a typical uphill reaction which needed additional energy to activate the reaction [64,65]. A suitable band alignment toward the water splitting and abundant electron/hole pairs forming become important issues. However, the H_2 evolution over all metal-H:TiO_2 NFs under visible light illumination is too low to be detected. The low energy and intensity of visible light cannot entirely excited the metal-H:TiO_2 NFs to further produce sufficient amounts of electron/hole pairs. To evaluate the photoenergy conversion efficiency, which can be identified that how much photoenergy converted to chemical energy stored in hydrogen for UV-A and UV-B photons, the general definition is described as following,

$$\text{Photo energy conversion efficiency (\%)} = \frac{\text{output energy of hydrogen evolved}}{\text{energy of incident light}} \quad (8)$$

The photoenergy conversion efficiency of Pd-H:TiO_2 NFs under UV-A irradiation and under UV-B irradiation are ~7.54% and ~11.35%, respectively. Herein, the brief conclusion according to as-presented results is that Pd-H:TiO_2 NFs and Pt-H:TiO_2 NFs under UV irradiation perform a strong ability to produce the hydrogen. It can be attributed that the same series of Pd and Pt at group 10 element of periodic table always shows the similar electron configuration and chemical properties such as suitable work function for TiO_2 heterojunction [4]. The theoretical work function of as-mentioned metals reported by previous literature were summarized in Table S1. As these metals are decorated on the surface of TiO_2, the Schottky barrier is formed on the interface. Typically, the barrier heights for TiO_2 NFs (χ = 3.90 eV) decorated with palladium (ϕ_{Pd} = 5.60 eV), platinum (ϕ_{Pt} = 5.70 eV), and nickel (ϕ_{Ni} = 5.15 eV) [66] might be 1.70 eV, 1.80 eV, and 1.25 eV, respectively. It is effective to promote the water splitting reaction and rectify the electron-hole recombination [4]. In addition, combining the advantages of surface defects on H:TiO_2 NFs and the metal-induced Schottky barrier, the flows of electron-hole pairs might be rectified and the electrons effectively migrate to metal. Therefore, both of Pd-H:TiO_2 and Pt-H:TiO_2 NFs reveal high hydrogen evolution rate.

To further investigate the charge dynamic in the metal-H:TiO_2, photoelectrochemical properties were studied by several ways including photo-assisted LSV, EIS and transient photocurrent measurement. Fig. 9 presents the EIS Nyquist plot of three kinds of TiO_2-based photocatalyst. Typically, the arc radius of EIS depicts the resistance of the interface layer on the electrode.[67,68] The small arc radius of all TiO_2 photocatalysts were found under irradiation, indicating that the lower resistance is due to the more production of charge carrier compared to the condition in the dark. Fig. 10a shows the photocurrent response in the dark and under UV irradiation over pristine TiO_2, H:TiO_2, and Pd-H:TiO_2. Under the UV irradiation, the photocurrent density of all TiO_2 electrodes exhibit a significant improvement, and Pd-H:TiO_2 presents the highest response. It is attributed to the metal decoration which could further enhance the light harvesting as well as

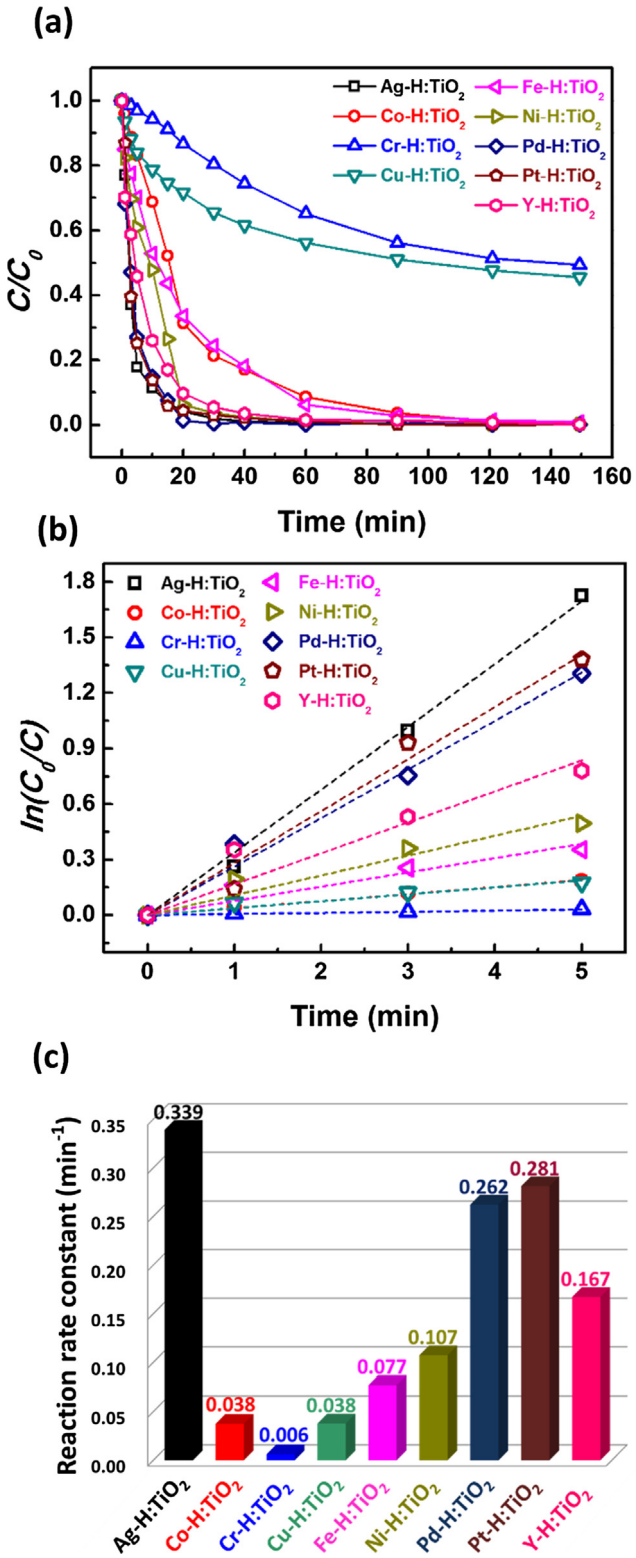

Fig. 7. (a) The C/C_o curves, (b) the linearized kinetic plots and (c) the reaction rate constants for the photodegradation of brilliant green using various metal-H:TiO_2 NFs.

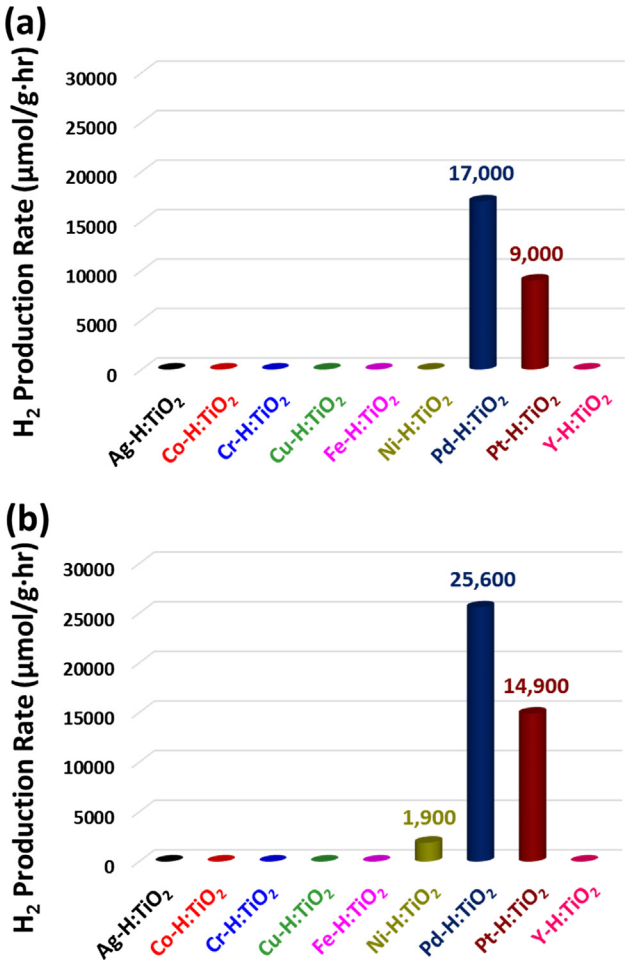

Fig. 8. The hydrogen evolution rates of various metal-H:TiO_2 NFs under the following light source illumination: (a) UV-A, and (b) UV-B.

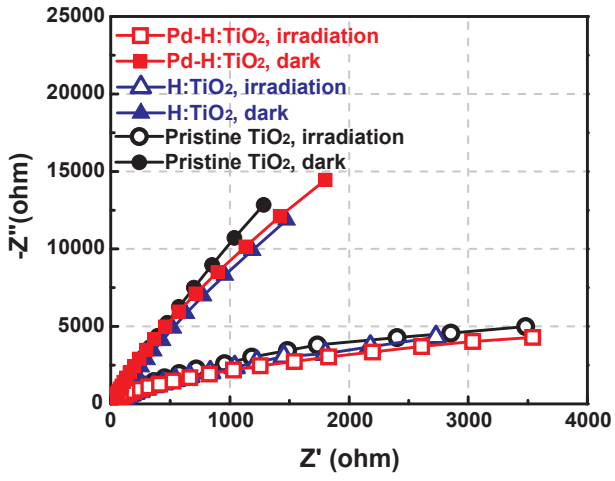

Fig. 9. EIS Nyquist plot of various TiO_2 in the dark and under the UV irradiation.

transport the charge efficiently.[67,68] According to Fig. 10b of transient photocurrent, the current density not only increased dramatically but also addressed the delay in the circuit when the transient photocurrent generated. Interestingly, H:TiO_2 promotes the electrons transfer to and retain on the surface defect (oxygen vacancy and Ti^{3+} interstitial defect) [60],which could further delay the photocurrent transition. Therefore, we believe that metal decoration is quite beneficial to charge transport and light harvesting, and demonstrate the superiority of Schottky barrier in the metal-H:TiO_2. The chemical state analysis of various TiO_2 catalyst analyzed by X-ray photoelectron spectroscopy (Fig. S2) suggested the more intense Ti^{3+} signal located around 457.8 eV in the H:TiO_2 and metal-H:TiO_2 owing to the Ti^{3+} interstitial

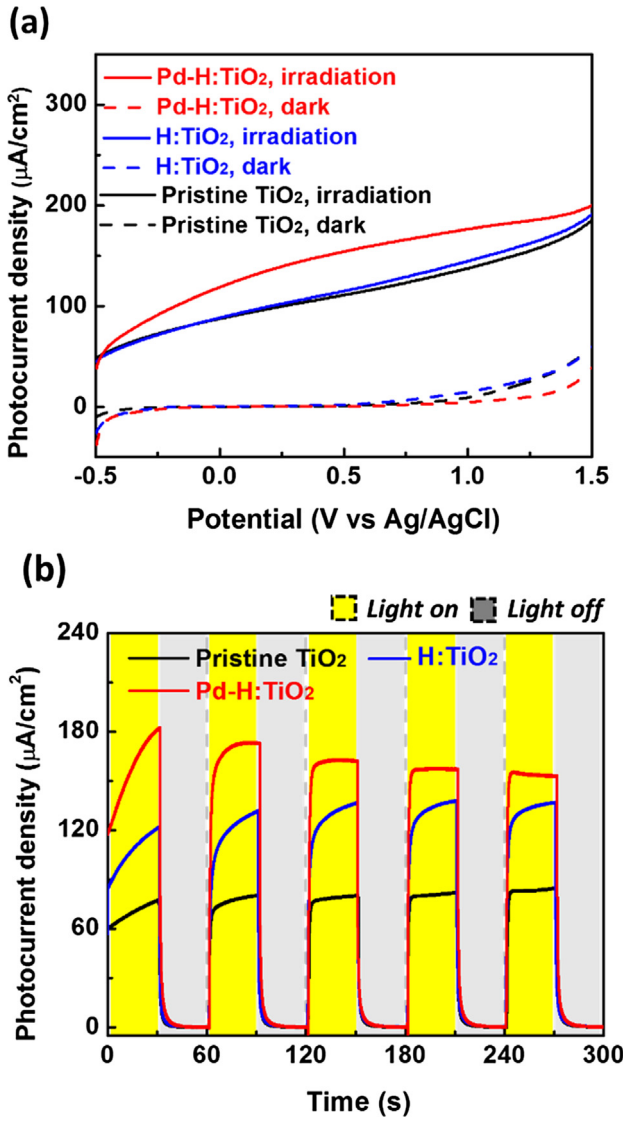

Fig. 10. (a) Photocurrent response measured by LSV of the pristine TiO_2, H:TiO_2, and Pd-H:TiO_2 in the dark and under UV-B irradiation. (b) Transient photocurrent of pristine TiO_2, H:TiO_2, and Pd-H:TiO_2 under UV-B irradiation.

defects.[60] In addition, the composition of palladium were about 0.49 at%. The BET specific surface area and the pore distribution were summarized in Fig. S3 and Table S2. Among three kinds TiO_2 photocatalyst, H:TiO_2 presents the largest surface area which is ~34.21 $m^2 \cdot g^{-1}$ because of much more surface defects. The surface area of Pd-H:TiO_2 remained 31.80 $m^2 \cdot g^{-1}$ suggested that these surface defects were overlaid by the metal nanoparticles which is about 5.0 nm, characterized by HRTEM as shown in Fig. S4.

The mechanism of photocatalytic hydrogen evolution from ethanol aqueous solution over various metal-H:TiO_2 NFs are illustrated in Fig. 11. Once the metal-H:TiO_2 NFs is illuminated by light, the photocatalytic reaction initiates. Photon with the sufficient energy intensity is capable to generate the photoexcited electron-hole pair. During the carrier migration processes, some of the photoexcited charges may recombine. To avoid the rapid recombination of electron-hole pair, the introduced surface defects provide trapping sites for photoexcited carriers. In the meanwhile, the separated hole would react with ethanol which acts as sacrificial agents to form proton which would further react with electron to generate H_2. In addition, the metal nanoparticles with the appropriate chemical states decorated on the surface of H:TiO_2 NFs acts as electron reservoirs to capture the photogenerated electron on TiO_2 and the electron subsequently react with proton to form hydrogen. With the cooperation of Schottky interface between TiO_2 and the metal nanoparticle, the large work function of metal nanoparticles could facilitate the electron that trapped by oxygen vacancy and Ti^{3+} interstitial defect to transport to the surface of metal nanoparticles. Furthermore, the existence of Schottky barrier could prevent the electron restricted in metal nanoparticle inject back to semiconductor. Therefore, we can expect that the metal-H:TiO_2 NFs possesses a more efficient charge separation and a lower electron-hole recombination rate [69].

4. Conclusion

Many types of metal nanoparticles were chosen to decorate on H:TiO_2 NFs surface to enhance the photodegradation activity and the photocatalytic hydrogen production rates. For each metal-H:TiO_2 NFs, the metal loading is ~1.0 wt%. For the photodegradation of organic dye, Ag-H:TiO_2 NFs shows the fastest decoloration phenomenon. For the photocatalytic hydrogen production, the highest hydrogen production rate was produced by Pd-H:TiO_2 NFs at a rate of ~17,000 μmol/g·h under UV-A irradiation and at ~25,600 μmol/g·h under UV-B irradiation corresponding to the photo energy conversion efficiency of ~7.54% and ~11.35%, respectively. Ag-H:TiO_2 NFs and

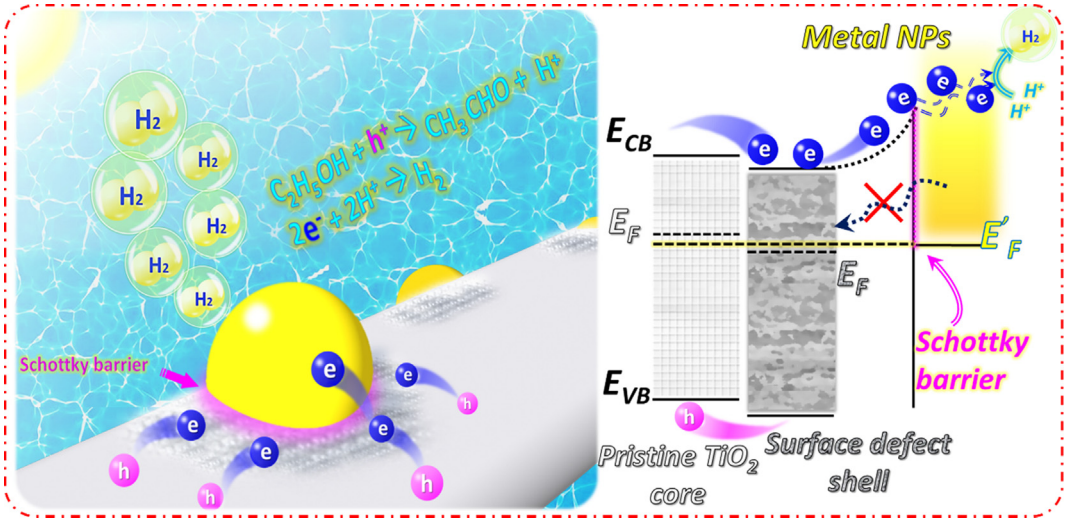

Fig. 11. The mechanism of photocatalytic hydrogen evolution from ethanol-water mixture over various metal-H:TiO_2 NFs.

Pd-H:TiO_2 NFs synthesized in our study represent the typical metal-semiconductor heterostructure systems that could be widely developed in this study can be a facile and environmentally friendly way for searching the high-performance photocatalysts in the field of environmental and energy issue.

Acknowledgements

The authors appreciate Miss Y.-M. Chang at Instrumentation Centre of National Tsing Hua University for TEM analysis. We would like to thank the financial support of Chang Gung Memorial Hospital, Linkou (Project No. CMRPD2H0171 and BMRPC74) and Ministry of Science and Technology, Taiwan (Project No. 107-2119-M-002-012 and 106-2221-E-182-057-MY3).

Appendix A. Supplementary material

Supplementary data to this article can be found online at https://doi.org/10.1016/j.apsusc.2018.10.240.

References

[1] D.V. Bavykin, J.M. Friedrich, F.C. Walsh, Protonated titanates and TiO_2 nanostructured materials: synthesis, properties, and applications, Adv. Mater. 18 (2006) 2807–2824.
[2] A.J. Nozik, Photoelectrolysis of water using semiconducting TiO_2 crystals, Nature 257 (1975) 383–386.
[3] M.-C. Wu, P.-H. Lee, D.-L. Lee, Enhanced photocatalytic activity of palladium decorated TiO_2 nanofibers containing anatase-rutile mixed phase, Int. J. Hydrogen Energy 40 (2015) 4558–4566.
[4] M.-C. Wu, A. Sápi, A. Avila, M. Szabó, J. Hiltunen, M. Huuhtanen, G. Tóth, Á. Kukovecz, Z. Kónya, R. Keiski, W.-F. Su, H. Jantunen, K. Kordás, Enhanced photocatalytic activity of TiO_2 nanofibers and their flexible composite films: decomposition of organic dyes and efficient H_2 generation from ethanol-water mixtures, Nano Res. 4 (2011) 360–369.
[5] M. Pelaez, N.T. Nolan, S.C. Pillai, M.K. Seery, P. Falaras, A.G. Kontos, P.S.M. Dunlop, J.W.J. Hamilton, J.A. Byrne, K. O'Shea, M.H. Entezari, D.D. Dionysiou, A review on the visible light active titanium dioxide photocatalysts for environmental applications, Appl. Catal., B 125 (2012) 331–349.
[6] C. Wang, D. Meng, J. Sun, J. Memon, Y. Huang, J. Geng, Graphene wrapped TiO_2 based catalysts with enhanced photocatalytic activity, Adv. Mater. Interfaces 1 (2014) 1300150.
[7] J. Low, C. Jiang, B. Cheng, S. Wageh, A.A. Al-Ghamdi, J. Yu, A Review of direct Z-scheme photocatalysts, Small Methods 1 (2017) 1700080.
[8] L. Yang, Y. Gao, F. Wang, P. Liu, S. Hu, Enhanced photocatalytic performance of cementitious material with TiO_2 @Ag modified fly ash micro-aggregates, Chin. J. Catal. 38 (2017) 357–364.
[9] K. Qi, B. Cheng, J. Yu, W. Ho, A review on TiO_2-based Z-scheme photocatalysts, Chin. J. Catal. 38 (2017) 1936–1955.
[10] J. Low, B. Cheng, J. Yu, Surface modification and enhanced photocatalytic CO_2 reduction performance of TiO_2: a review, Appl. Surf. Sci. 392 (2017) 658–686.
[11] F. Xu, J. Zhang, B. Zhu, J. Yu, J. Xu, $CuInS_2$ sensitized TiO_2 hybrid nanofibers for improved photocatalytic CO_2 reduction, Appl. Catal., B 230 (2018) 194–202.
[12] A. Meng, J. Zhang, D. Xu, B. Cheng, J. Yu, Enhanced photocatalytic H_2-production activity of anatase TiO_2 nanosheet by selectively depositing dual-cocatalysts on 101 and 001 facets, Appl. Catal., B 198 (2016) 286–294.
[13] L. Zheng, X. Yu, M. Long, Q. Li, Humic acid-mediated visible-light degradation of phenol on phosphate-modified and Nafion-modified TiO_2 surfaces, Chin. J. Catal. 38 (2017) 2076–2084.
[14] S. Chuangchote, J. Jitputti, T. Sagawa, S. Yoshikawa, Photocatalytic activity for hydrogen evolution of electrospun TiO_2 nanofibers, ACS Appl. Mater. Interfaces 1 (2009) 1140–1143.
[15] T.P. Feist, P.K. Davies, The soft chemical synthesis of TiO_2 (B) from layered titanates, J. Solid State Chem. 101 (1992) 275–295.
[16] E. Horváth, Á. Kukovecz, Z. Kónya, I. Kiricsi, Hydrothermal conversion of self-assembled titanate nanotubes into nanowires in a revolving autoclave, Chem. Mater. 19 (2007) 927–931.
[17] Z.R. Tian, J.A. Voigt, J. Liu, B. McKenzie, H. Xu, Large Oriented arrays and continuous films of TiO_2-based nanotubes, J. Am. Chem. Soc. 125 (2003) 12384–12385.
[18] Y. Wang, G. Du, H. Liu, D. Liu, S. Qin, N. Wang, C. Hu, X. Tao, J. Jiao, J. Wang, Z.L. Wang, Nanostructured sheets of Ti-O nanobelts for gas sensing and antibacterial applications, Adv. Funct. Mater. 18 (2008) 1131–1137.
[19] P. Zhang, S. Yin, V. Petrykin, M. Kakihana, T. Sato, Preparation of high performance fibrous titania photocatalysts by the solvothermal reaction of protonated form of tetratitanate, J. Mol. Catal. A: Chem. 309 (2009) 50–56.
[20] S. Zhang, Q. Chen, L.M. Peng, Structure and formation of $H_2Ti_3O_7$ nanotubes in an alkali environment, Phys. Rev. B 71 (2005) 014104.
[21] F. Xu, W. Xiao, B. Cheng, J. Yu, Direct Z-scheme anatase/rutile bi-phase nanocomposite TiO_2 nanofiber photocatalyst with enhanced photocatalytic H_2-production activity, Int. J. Hydrogen Energy 39 (2014) 15394–15402.
[22] Y. Shi, D. Yang, Y. Li, J. Qu, Z.-Z. Yu, Fabrication of PAN@TiO_2/Ag nanofibrous membrane with high visible light response and satisfactory recyclability for dye photocatalytic degradation, Appl. Surf. Sci. 426 (2017) 622–629.
[23] D. Wang, Y. Liu, C. Wang, F. Zhou, W. Liu, Highly flexible coaxial nanohybrids made from porous TiO_2 Nanotubes, ACS Nano 3 (2009) 1249–1257.
[24] K. Woan, G. Pyrgiotakis, W. Sigmund, Photocatalytic carbon-nanotube–TiO_2 composites, Adv. Mater. 21 (2009) 2233–2239.
[25] F. Tian, D. Hou, F. Hu, K. Xie, X. Qiao, D. Li, Pouous TiO_2 nanofibers decorated CdS nanoparticles by SILAR method for enhanced visible-light-driven photocatalytic activity, Appl. Surf. Sci. 391 (2017) 295–302.
[26] H. Li, T. Zhang, C. Pan, C. Pu, Y. Hu, X. Hu, E. Liu, J. Fan, Self-assembled Bi_2MoO_6/TiO_2 nanofiber heterojunction film with enhanced photocatalytic activities, Appl. Surf. Sci. 391 (2017) 303–310.
[27] S.I. Boyadjiev, O. Kéri, P. Bárdos, T. Firkala, F. Gáber, Z.K. Nagy, Z. Baji, M. Takács, I.M. Szilágyi, TiO_2/ZnO and ZnO/TiO_2 core/shell nanofibers prepared by electrospinning and atomic layer deposition for photocatalysis and gas sensing, Appl. Surf. Sci. 424 (2017) 190–197.
[28] X. Chen, L. Liu, F. Huang, Black titanium dioxide (TiO_2) nanomaterials, Chem. Soc. Rev. 44 (2015) 1861–1885.
[29] X. Chen, L. Liu, Z. Liu, M.A. Marcus, W.-C. Wang, N.A. Oyler, M.E. Grass, B. Mao, P.-A. Glans, P.Y. Yu, J. Guo, S.S. Mao, Properties of disorder-engineered black titanium dioxide nanoparticles through hydrogenation, Sci. Rep. 3 (2013) 1510.
[30] E. Binetti, Z. El Koura, N. Patel, A. Dashora, A. Miotello, Rapid hydrogenation of amorphous TiO_2 to produce efficient H-doped anatase for photocatalytic water splitting, Appl. Catal., A 500 (2015) 69–73.
[31] Y. Yan, M. Han, A. Konkin, T. Koppe, D. Wang, T. Andreu, G. Chen, U. Vetter, J.R. Morante, P. Schaaf, Slightly hydrogenated TiO_2 with enhanced photocatalytic performance, J. Mater. Chem. A 2 (2014) 12708–12716.
[32] S. Zhang, S. Zhang, B. Peng, H. Wang, H. Yu, H. Wang, F. Peng, High performance hydrogenated TiO_2 nanorod arrays as a photoelectrochemical sensor for organic compounds under visible light, Electrochem. Commun. 40 (2014) 24–27.
[33] H. Cui, W. Zhao, C. Yang, H. Yin, T. Lin, Y. Shan, Y. Xie, H. Gu, F. Huang, Black TiO_2 nanotube arrays for high-efficiency photoelectrochemical water-splitting, J. Mater. Chem. A 2 (2014) 8612–8616.
[34] G. Wang, H. Wang, Y. Ling, Y. Tang, X. Yang, R.C. Fitzmorris, C. Wang, J.Z. Zhang, Y. Li, Hydrogen-treated TiO_2 nanowire arrays for photoelectrochemical water splitting, Nano Lett. 11 (2011) 3026–3033.
[35] L. Liu, P.Y. Yu, X. Chen, S.S. Mao, D.Z. Shen, hydrogenation and disorder in engineered black TiO_2, Phys. Rev. Lett. 111 (2013) 065505.
[36] J. Cai, Z.a. Huang, K. Lv, J. Sun, K. Deng, Ti powder-assisted synthesis of Ti^{3+} self-doped TiO_2 nanosheets with enhanced visible-light photoactivity, RSC Adv. 4 (2014) 19588–19593.
[37] X. Wang, S. Zhang, Y. Xie, H. Wang, H. Yu, Y. Shen, Z. Li, S. Zhang, F. Peng, Branched hydrogenated TiO_2 nanorod arrays for improving photocatalytic hydrogen evolution performance under simulated solar light, Int. J. Hydrogen Energy 41 (2016) 20192–20197.
[38] L. Hou, M. Zhang, Z. Guan, Q. Li, J. Yang, Effect of annealing ambience on the formation of surface/bulk oxygen vacancies in TiO_2 for photocatalytic hydrogen evolution, Appl. Surf. Sci. 428 (2018) 640–647.
[39] J. Tian, Y. Leng, H. Cui, H. Liu, Hydrogenated TiO_2 nanobelts as highly efficient photocatalytic organic dye degradation and hydrogen evolution photocatalyst, J Hazard Mater 299 (2015) 165–173.
[40] E.M. Samsudin, S.B.A. Hamid, J.C. Juan, W.J. Basirun, A.E. Kandjani, Surface modification of mixed-phase hydrogenated TiO_2 and corresponding photocatalytic response, Appl. Surf. Sci. 359 (2015) 883–896.
[41] D. Li, J. Jia, T. Zheng, X. Cheng, X. Yu, Construction and characterization of visible light active Pd nano-crystallite decorated and C-N-S-co-doped TiO_2 nanosheet array photoelectrode for enhanced photocatalytic degradation of acetylsalicylic acid, Appl. Catal., B 188 (2016) 259–271.
[42] A. Gołąbiewska, A. Malankowska, M. Jarek, W. Lisowski, G. Nowaczyk, S. Jurga, A. Zaleska-Medynska, The effect of gold shape and size on the properties and visible light-induced photoactivity of Au-TiO_2, Appl. Catal., B 196 (2016) 27–40.
[43] Y. Huang, Q. Shang, D. Wang, S. Yang, H. Guan, Q. Lu, S.C. Tsang, Effects of electronic structure and interfacial interaction between metal-quinoline complexes and TiO_2 on visible light photocatalytic activity of TiO_2, Appl. Catal., B 187 (2016) 59–66.
[44] B. Cao, G. Li, H. Li, Hollow spherical RuO_2@TiO_2@Pt bifunctional photocatalyst for coupled H_2 production and pollutant degradation, Appl. Catal., B 194 (2016) 42–49.
[45] M.-C. Wu, J. Hiltunen, A. Sápi, A. Avila, W. Larsson, H.-C. Liao, M. Huuhtanen, G. Tóth, A. Shchukarev, N. Laufer, Á. Kukovecz, Z. Kónya, J.-P. Mikkola, R. Keiski, W.-F. Su, Y.-F. Chen, H. Jantunen, P.M. Ajayan, R. Vajtai, K. Kordás, Nitrogen-doped anatase nanofibers decorated with noble metal nanoparticles for photocatalytic production of hydrogen, ACS Nano 5 (2011) 5025–5030.
[46] Y. Wang, J. Yu, W. Xiao, Q. Li, Microwave-assisted hydrothermal synthesis of graphene based Au–TiO_2 photocatalysts for efficient visible-light hydrogen production, J. Mater. Chem. A 2 (2014) 3847–3855.
[47] E. Aguiló, L. Soler, A. Casanovas, A.J. Moro, J.C. Lima, L. Rodríguez, J. Llorca, Gold (I)-complex-titania hybrid photocatalyst for hydrogen production, ChemCatChem 9 (2017) 3289–3292.
[48] J.B. Priebe, J. Radnik, C. Kreyenschulte, A.J.J. Lennox, H. Junge, M. Beller, A. Brückner, H_2 generation with (mixed) plasmonic Cu/Au-TiO_2 photocatalysts: structure-reactivity relationships assessed by in situ spectroscopy, ChemCatChem 9 (2017) 1025–1031.

[49] C. Jin, Y. Dai, W. Wei, X. Ma, M. Li, B. Huang, Effects of single metal atom (Pt, Pd, Rh and Ru) adsorption on the photocatalytic properties of anatase TiO_2, Appl. Surf. Sci. 426 (2017) 639–646.
[50] L. Kong, X. Zhang, C. Wang, F. Wan, L. Li, Synergic effects of Cu_xO electron transfer co-catalyst and valence band edge control over TiO_2 for efficient visible-light photocatalysis, Chin. J. Catal. 38 (2017) 2120–2131.
[51] S. Cao, H. Li, Y. Li, B. Zhu, J. Yu, Dependence of exposed facet of Pd on photocatalytic H_2-production activity, ACS Sustain. Chem. Eng. 6 (2018) 6478–6487.
[52] A. Busiakiewicz, A. Kisielewska, I. Piwoński, D. Batory, The effect of Fe segregation on the photocatalytic growth of Ag nanoparticles on rutile TiO_2 (001), Appl. Surf. Sci. 401 (2017) 378–384.
[53] J. Yu, L. Qi, M. Jaroniec, Hydrogen production by photocatalytic water splitting over Pt/TiO_2 nanosheets with exposed (001) facets, J. Phys. Chem. C 114 (2010) 13118–13125.
[54] Z. Yang, J. Lu, W. Ye, C. Yu, Y. Chang, Preparation of Pt/TiO_2 hollow nanofibers with highly visible light photocatalytic activity, Appl. Surf. Sci. 392 (2017) 472–480.
[55] H. Liang, Z. Jia, H. Zhang, X. Wang, J. Wang, Photocatalysis oxidation activity regulation of Ag/TiO_2 composites evaluated by the selective oxidation of Rhodamine B, Appl. Surf. Sci. 422 (2017) 1–10.
[56] J. Singh, K. Sahu, A. Pandey, M. Kumar, T. Ghosh, B. Satpati, T. Som, S. Varma, D.K. Avasthi, S. Mohapatra, Atom beam sputtered Ag-TiO_2 plasmonic nanocomposite thin films for photocatalytic applications, Appl. Surf. Sci. 411 (2017) 347–354.
[57] F. Bensouici, M. Bououdina, A.A. Dakhel, R. Tala-Ighil, M. Tounane, A. Iratni, T. Souier, S. Liu, W. Cai, Optical, structural and photocatalysis properties of Cu-doped TiO_2 thin films, Appl. Surf. Sci. 395 (2017) 110–116.
[58] M.-C. Wu, P.-Y. Wu, T.-H. Lin, T.-F. Lin, Photocatalytic performance of Cu-doped TiO_2 nanofibers treated by the hydrothermal synthesis and air-thermal treatment, Appl. Surf. Sci. 430 (2018) 390–398.
[59] M.-C. Wu, I.C. Chang, W.-K. Huang, Y.-C. Tu, C.-P. Hsu, W.-F. Su, Correlation between palladium chemical state and photocatalytic performance of TiO_2–Pd based nanoparticles, Thin Solid Films 570 (2014) 371–375.
[60] M.-C. Wu, C.-H. Chen, W.-K. Huang, K.-C. Hsiao, T.-H. Lin, S.-H. Chan, P.-Y. Wu, C.-F. Lu, Y.-H. Chang, T.-F. Lin, K.-H. Hsu, J.-F. Hsu, K.-M. Lee, J.-J. Shyue, K. Kordás, W.-F. Su, Improved solar-driven photocatalytic performance of highly crystalline hydrogenated tio_2 nanofibers with core-shell structure, Sci. Rep. 7 (2017) 40896.
[61] J. Zhang, M. Li, Z. Feng, J. Chen, C. Li, UV Raman spectroscopic study on TiO_2. I. phase transformation at the surface and in the bulk, J. Phys. Chem. B 110 (2006) 927–935.
[62] A. Katti, S.R. Venna, M.A. Carreon, Self-assembly hydrothermal assisted synthesis of mesoporous anatase in the presence of ethylene glycol, Catal. Commun. 10 (2009) 2036–2040.
[63] J. Schneider, M. Matsuoka, M. Takeuchi, J. Zhang, Y. Horiuchi, M. Anpo, D.W. Bahnemann, Understanding TiO_2 photocatalysis: mechanisms and materials, Chem. Rev. 114 (2014) 9919–9986.
[64] J. Wen, X. Li, W. Liu, Y. Fang, J. Xie, Y. Xu, Photocatalysis fundamentals and surface modification of TiO_2 nanomaterials, Chin. J. Catal. 36 (2015) 2049–2070.
[65] A. Kudo, Y. Miseki, Heterogeneous photocatalyst materials for water splitting, Chem. Soc. Rev. 38 (2009) 253–278.
[66] H.B. Michaelson, The work function of the elements and its periodicity, J. Appl. Phys. 48 (1977) 4729–4733.
[67] M.M. Khan, S.A. Ansari, D. Pradhan, M.O. Ansari, D.H. Han, J. Lee, M.H. Cho, Band gap engineered TiO_2 nanoparticles for visible light induced photoelectrochemical and photocatalytic studies, J. Mater. Chem. A 2 (2014) 637–644.
[68] X. Bai, L. Wang, R. Zong, Y. Lv, Y. Sun, Y. Zhu, Performance enhancement of ZnO photocatalyst via synergic effect of surface oxygen defect and graphene hybridization, Langmuir 29 (2013) 3097–3105.
[69] Z. Xu, Y. Lin, M. Yin, H. Zhang, C. Cheng, L. Lu, X. Xue, H.J. Fan, X. Chen, D. Li, Understanding the Enhancement mechanisms of surface plasmon-mediated photoelectrochemical electrodes: a case study on Au nanoparticle decorated TiO_2 nanotubes, Adv. Mater. Interfaces 2 (2015) 1500169.